Spontaneous Edge Accumulation of Spin Currents in Finite-Size Two-Dimensional Diffusive Spin-Orbit Coupled SFS Heterostructures

Mohammad Alidoust[1,2,*] and Klaus Halterman[3,†]

[1]*Department of Physics, University of Basel, Klingelbergstrasse 82, CH-4056 Basel, Switzerland*
[2]*Department of Physics, Faculty of Sciences, University of Isfahan, Hezar Jerib Avenue, Isfahan 81746-73441, Iran*
[3]*Michelson Lab, Physics Division, Naval Air Warfare Center, China Lake, California 93555, USA*

(Dated: April 24, 2015)

We theoretically study spin and charge currents through finite-size two-dimensional s-wave superconductor/uniform ferromagnet/s-wave superconductor ($S/F/S$) junctions with intrinsic spin-orbit interactions (ISOIs) using a quasiclassical approach. Considering experimentally realistic parameters, we demonstrate that the combination of spontaneously broken time-reversal symmetry and lack of inversion symmetry can result in spontaneously accumulated spin currents at the edges of finite-size two-dimensional magnetic S/F hybrids. Due to the spontaneous edge spin accumulation, the corners of the F wire host the maximum spin current density. We further reveal that this type edge phenomena are robust and independent of either the actual type of ISOIs or exchange field orientation. Moreover, we study spin current-phase relations in these diffusive spin-orbit coupled $S/F/S$ junctions. Our results unveil net spin currents, not accompanied by charge supercurrent, that spontaneously accumulate at the sample edges through a modulating superconducting phase difference. Finally, we discuss possible experimental implementations to observe these edge phenomena.

PACS numbers: 74.50.+r, 74.45.+c, 74.25.Ha, 74.78.Na

I. INTRODUCTION

Spintronics devices operate by spin transport mechanisms[1–6] rather than by utilizing charged carriers, as is done typically in conventional electronics devices. The use of spin currents can result in higher speeds and reduced dissipation[2,6] while exhibiting weak sensitivity to nonmagnetic impurities and temperature.[4–6] For functional spin-based devices, it is necessary to manipulate and generate spin-currents in a practical and efficient manner. For this reason, many investigations have focused on harnessing the spin-orbit interactions[12,13] (SOIs) present in many materials, including semiconductors.[7–11,14–17] The SOI is a quantum relativistic phenomenon that can be divided into two categories: i) intrinsic (originating from the electronic band structure of the material) and ii) extrinsic (originating from spin-dependent scattering of impurities).[4–6] The intrinsic spin-orbit interactions (ISOIs) such as Rashba[12] and Dresselhaus[13], are experimentally controllable via tuning a gate voltage[16,18–24]. This particular attribute has proliferated efforts striving for high-performance spin-based devices, including transistors, and new routes in information storage and transport.[3,15,16,20,25–27] Similarly, ferromagnet (F) and superconductor (S) heterostructures have received renewed interest lately due to the possibility of generating spin polarized triplet supercurrents[28–37] that can be used for practical purposes[32]. By considering a ferromagnet with an ISOI, the spin orbit interaction can couple with the magnetic exchange field, resulting in modified superconducting proximity effects and additional venues for new spin phenomena. Indeed, the ISOI can induce long-range proximity effects in uniformly magnetized S/F structures due to the momentum-dependence of the effective exchange field[73]. It is therefore of fundamental importance not only to find a simple, experimentally accessible structure that can support spin currents in F/S systems, but it is also crucial to determine the spatial behavior of the spin currents near the boundaries of the superconducting hybrids.

Many past works are based on the application of *external* electric or magnetic fields. One of the earliest such cases involved the combination of SOIs and an external electric field, giving rise to an accumulation of spin currents at the edges[41,42] (the so called spin-Hall effect[39,40]). The spin currents generally tend to peak near the sample boundaries and vanish at the electrode/sample interfaces.[44–47] These theoretical predictions were later experimentally observed in semiconductor samples[43]. The spin-Hall phenomenon was also extensively studied in superconducting heterostructures where various types of spin-orbit coupling (SOC) play key roles.[23,50–67] For example, the out-of-plane component of the spin density was theoretically investigated[50] in a spin-orbit coupled $S/N/S$ junction [with normal metal (N) interlayer] subject to an inhomogeneous external magnetic field. It was found that the spin density varies along the transverse direction, leading to a longitudinal phase difference between the S electrodes. The influence of extrinsic SOIs on the critical supercurrent in diffusive magnetic hybrid structures was also studied.[71,72] In nonmagnetic $S/N/S$ Josephson junctions with SOC subject to a magnetic field, 0-π transitions may be induced.[29] In an earlier work[74], singlet-triplet pair conversion was numerically investigated using a lattice model in a ballistic half metal ferromagnetic Josephson junction with an interfacial Rashba SOC. Several optimal configurations have also been theoretically studied for generating and detecting the predicted long-range triplet correlations in experiments.[73]

In this paper, we study the local spin currents in uniformly magnetized $S/F/S$ Josephson junctions with spatially uniform intrinsic SOIs, avoiding any external electric or magnetic fields. We employ a two-dimensional quasiclassical Keldysh-Usadel approach that incorporates a generic spin-dependent vector potential to study the behavior of the spin current components. We consider two types of ISOCs: i) Rashba and

ii) Dresselhaus SOC, and the magnetization of the F wire can take arbitrary orientations. We find that the coupling of the F wire's exchange field and ISOIs leads to edge spin currents with three nonzero components. The spin current density components peak near the edges of the F strip and sharply decline when moving away from the edges. Therefore, the maximal spin current accumulation takes place near the F wire's corners. This phenomenon can be also observed in ISO coupled $S/N/S$ junctions with a single spin active N/S interface as demonstrated in Ref. 75. Our results show that the spin current can be switched on or off at the S/F contacts, depending on the magnetization direction. The spatially averaged spin current components reveal a 2π-periodicity and even-functionality in φ, the phase difference between the S terminals. This is in contrast to the charge supercurrent which is a 2π-periodic odd function of φ (and consistent with previous studies[68]). Note that for such junctions, the argument in the current phase relation for some situations can become modified by a simple φ_0 shift.[66,69,70]

The simple hybrid structure proposed here relies solely on the intrinsic properties of the system, in contrast to other structures that rely inextricably on external fields to observe the edge spin currents[39–46,49,50,67]. Our device consists of a finite-size intrinsic SO coupled F wire (with uniform magnetization) sandwiched between two S banks. The spin currents then spontaneously accumulate at the sample edges, *without* the application of an external electric or magnetic field to the system. We demonstrate that the device allows for the realization of spin currents in the *absence* of charge supercurrent by simply modulating φ. The edge spin accumulation is a signature of the spin Hall effect[67], and hence can be experimentally measured by optical experiments for instance[43] (see the discussions in Sec. III). Also, we discuss the symmetries present among the spin current components when varying the magnetization orientation with Rashba or Dresselhaus SOC present. Moreover, we compare our results with the charge and spin currents found in a nonmagnetic diffusive $S/N/S$ Josephson junction with Rashba and/or Dresselhaus SOC. We find that the spin currents vanish in the $S/N/S$ devices, consistent with previous works[67,75], and that the charge current displays a spatially uniform profile without any transverse component, indicating conservation of charge current.

The paper is organized as follows. We outline the theoretical framework used to study hybrid structures with ISOCs in Sec. II. In Sec. III, the results of diffusive $S/F/S$ Josephson junctions are presented for the case of Rashba ISOC. We next utilize the symmetries in the spin currents to give a simple prescription for finding the corresponding results for the Dresselhaus spin-orbit interaction. We finally present concluding remarks in Sec. IV.

II. THEORETICAL FORMALISM

The intrinsic SOI is a consequence of the moving carriers' spin interaction with an atomic potential $V(\boldsymbol{r})$. Therefore, the total Hamiltonian of a moving electron in such an atomic potential can be expressed as,[20,76]

$$\mathbb{H} = \frac{\vec{\mathcal{P}}^2}{2m} + \frac{e\hbar^2}{4m_0^2c^2}\vec{\mathcal{P}}\cdot\Big\{\vec{\tau}\times\vec{\partial}V(\boldsymbol{r})\Big\}, \tag{1}$$

where $m_0 = 0.51$Mev, is the free electron mass and and c is the velocity of light in vacuum. We define $\vec{\mathcal{P}}$ to represent the electron's momentum vector, and $\vec{\partial} \equiv (\partial_x, \partial_y, \partial_z)$. The vector of Pauli matrices, $\vec{\tau}$, is given in Appendix A. It has been shown that the linearized SOC term can be simply accounted for as an effective background field that follows SU(2) gauge symmetries.[47,73,77,78] Hence, it is sufficient to replace partial derivatives, appearing in the quasiclassical formalism, by their covariants.[47,73] Another advantage of the SU(2) approach is the convenient definition of physical quantities such as spin currents.[79]

We start with the Usadel equations that enable us to study the charge and spin transport through diffusive F/S systems with the ferromagnetic regions having arbitrary magnetization patterns $\vec{h}(\boldsymbol{r}) = \big(h^x(\boldsymbol{r}), h^y(\boldsymbol{r}), h^z(\boldsymbol{r})\big)$:[28,73,80]

$$\Big[\hat{\partial}, \hat{G}(\boldsymbol{r})[\hat{\partial}, \hat{G}(\boldsymbol{r})]\Big] = \frac{-i}{D}\Big[\varepsilon\hat{\rho}_3 + \mathrm{diag}[\mathcal{H}(\boldsymbol{r}), \mathcal{H}^{\mathcal{T}}(\boldsymbol{r})], \hat{G}(\boldsymbol{r})\Big], \tag{2}$$

$$\mathcal{H}(\boldsymbol{r}) = \vec{h}(\boldsymbol{r})\cdot\vec{\sigma},$$

where $\vec{\hat{\rho}}$ and $\vec{\sigma}$ denote vectors comprised of 4×4 and 2×2 Pauli matrices (see Appendix A), and D represents the diffusive constant of the ferromagnetic medium. We have denoted the quasiparticles' energy by ε which is measured from the Fermi surface ε_F. Throughout this work, we focus on the low proximity limit of the diffusive regime[28]. In this limit, the normal and anomalous components of the Green's function can be approximated by, $\underline{F}^{no}(\boldsymbol{r}) \simeq \underline{1}$ and $\underline{F}(\boldsymbol{r}) \ll \underline{1}$, respectively. Thus, the advanced component of total Green's function, $\hat{G}(\boldsymbol{r})$, takes the following form:

$$\hat{G}^A(\boldsymbol{r},\varepsilon) \approx \begin{pmatrix} -\underline{1} & -\underline{F}(\boldsymbol{r},-\varepsilon) \\ \underline{F}^*(\boldsymbol{r},\varepsilon) & \underline{1} \end{pmatrix}, \tag{3}$$

where each entry stands for a 2×2 matrix block. Considering the Taylor expansion, the advanced component can be given by:

$$\hat{G}^A(\boldsymbol{r},\varepsilon) = \begin{pmatrix} -1 & 0 & -f_{\uparrow\uparrow}(\boldsymbol{r},-\varepsilon) & -f_{-}(\boldsymbol{r},-\varepsilon) \\ 0 & -1 & -f_{+}(\boldsymbol{r},-\varepsilon) & -f_{\downarrow\downarrow}(\boldsymbol{r},-\varepsilon) \\ f^*_{\uparrow\uparrow}(\boldsymbol{r},\varepsilon) & f^*_{-}(\boldsymbol{r},\varepsilon) & 1 & 0 \\ f^*_{+}(\boldsymbol{r},\varepsilon) & f^*_{\downarrow\downarrow}(\boldsymbol{r},\varepsilon) & 0 & 1 \end{pmatrix}. \tag{4}$$

Here we restrict our calculations to the equilibrium situations where the Retarded and Keldysh blocks of total Green's function are obtained by: $\hat{G}^A(\boldsymbol{r}) = -\big\{\hat{\rho}_3\hat{G}^R(\boldsymbol{r})\hat{\rho}_3\big\}^\dagger$, and $\hat{G}^K(\boldsymbol{r}) = \tanh(\varepsilon k_BT/2)\big\{\hat{G}^R(\boldsymbol{r}) - \hat{G}^A(\boldsymbol{r})\big\}$. Here, k_B and T denote the Boltzmann constant and system temperature, respectively.

The Usadel equation, Eq. (2), leads to sixteen coupled complex partial differential equations in the low proximity limit

that become highly complicated with the presence of intrinsic SOI terms. Unfortunately, the resultant system of coupled differential equations can only be simplified and decoupled under very limiting conditions,[28,29] leading to analytical results. However, for the systems considered in this paper, numerical methods are the most appropriate, and often the only possible routes to investigate the relevant transport properties.[73] The differential equations must be supplemented by the appropriate boundary conditions to properly capture the transport characteristics of $S/F/S$ hybrid structures. We thus employ the Kupriyanov-Lukichev boundary conditions at the S/F interfaces[81] and control the intensity of induced proximity correlations using the barrier resistance parameter, ζ:

$$\zeta\{\hat{G}(\boldsymbol{r})\hat{\partial}\hat{G}(\boldsymbol{r})\}\cdot\hat{\boldsymbol{n}}=[\hat{G}_{\rm BCS}(\theta),\hat{G}(\boldsymbol{r})], \tag{5}$$

where $\hat{\boldsymbol{n}}$ is a unit vector, directed perpendicular to a given interface. The solutions to Eqs. (2) for a bulk, even-frequency s-wave superconductor reads,

$$\hat{G}^R_{\rm BCS}(\theta)=\begin{pmatrix}\underline{1}\cosh\vartheta(\varepsilon) & i\sigma_2e^{i\theta}\sinh\vartheta(\varepsilon)\\ i\sigma_2e^{-i\theta}\sinh\vartheta(\varepsilon) & -\underline{1}\cosh\vartheta(\varepsilon)\end{pmatrix}, \tag{6}$$

in which,

$$\vartheta(\varepsilon)=\text{arctanh}(\frac{|\,\Delta\,|}{\varepsilon}),$$

is defined in terms of the superconducting gap Δ. Here the macroscopic phase of the bulk superconductor is denoted by θ, so that the difference between the macroscopic phases of the left and right S electrodes are given by $\theta_l-\theta_r=\varphi$. For more compact expressions in our subsequent calculations, we define the following piecewise functions:

$$s(\varepsilon)\equiv e^{i\theta}\sinh\vartheta(\varepsilon)=$$
$$-\Delta\left\{\frac{\text{sgn}(\varepsilon)}{\sqrt{\varepsilon^2-\Delta^2}}\Theta(\varepsilon^2-\Delta^2)-\frac{i}{\sqrt{\Delta^2-\varepsilon^2}}\Theta(\Delta^2-\varepsilon^2)\right\},$$
$$c(\varepsilon)\equiv\cosh\vartheta(\varepsilon)=$$
$$\frac{|\,\varepsilon\,|}{\sqrt{\varepsilon^2-\Delta^2}}\Theta(\varepsilon^2-\Delta^2)-\frac{i\varepsilon}{\sqrt{\Delta^2-\varepsilon^2}}\Theta(\Delta^2-\varepsilon^2),$$

where $\Theta(x)$ stands for the usual step function. It is clear that the general boundary conditions given by Eq. (5) do not permit current flow through the hard wall boundaries of the finite-size two-dimensional $S/F/S$ Josephson junction, shown in Fig. 1.

To study the influence of differing types of ISOI on the system transport characteristics, we adopt a spin-dependent tensor vector potential $\vec{A}(\boldsymbol{r})=\big(A_x(\boldsymbol{r}),A_y(\boldsymbol{r}),A_z(\boldsymbol{r})\big)$, as follows:[47,73,75,77,78]

$$A_x(\boldsymbol{r})=\frac{1}{2}\Big\{\mathcal{A}^x_x(\boldsymbol{r})\tau^x+\mathcal{A}^y_x(\boldsymbol{r})\tau^y+\mathcal{A}^z_x(\boldsymbol{r})\tau^z\Big\}, \tag{7a}$$
$$A_y(\boldsymbol{r})=\frac{1}{2}\Big\{\mathcal{A}^x_y(\boldsymbol{r})\tau^x+\mathcal{A}^y_y(\boldsymbol{r})\tau^y+\mathcal{A}^z_y(\boldsymbol{r})\tau^z\Big\}, \tag{7b}$$
$$A_z(\boldsymbol{r})=\frac{1}{2}\Big\{\mathcal{A}^x_z(\boldsymbol{r})\tau^x+\mathcal{A}^y_z(\boldsymbol{r})\tau^y+\mathcal{A}^z_z(\boldsymbol{r})\tau^z\Big\}. \tag{7c}$$

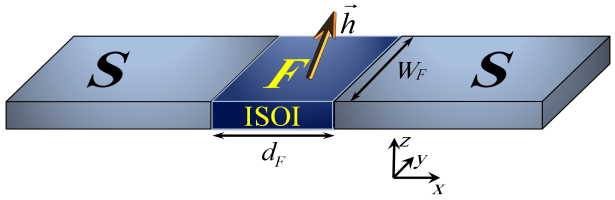

FIG. 1. (Color online) Schematic of a finite-size two-dimensional magnetic $S/F/S$ Josephson junction. The superconducting electrodes and rectangular ferromagnetic nano-wire are labelled S and F, respectively. We assume that the quasiparticle current experiences an intrinsic spin-orbit interaction (ISOI) solely inside the F region. The thickness and width of the ferromagnetic strip are labeled d_F and W_F, respectively. The junction is located in the xy plane and the S/F interfaces are along the y axis. The F region has a uniform exchange field denoted by $\vec{h}$ and can take arbitrary orientations $\big(h^x,h^y,h^z\big)$.

Using the above vector potential, we define the covariant derivatives by;

$$\hat{\partial}\equiv\vec{\partial}\hat{1}-ie\vec{A}(\boldsymbol{r}). \tag{8}$$

Accordingly, the brackets seen in the Usadel equation, Eq. (2), and the boundary conditions, Eq. (5), (as well as the charge and spin currents that shall be discussed below, Eqs. (10) and (11)) take the following form:

$$[\hat{\partial},\hat{G}(\boldsymbol{r})]=\vec{\partial}\hat{G}(\boldsymbol{r})-ie[\vec{A}(\boldsymbol{r}),\hat{G}(\boldsymbol{r})]. \tag{9}$$

The spin and charge currents are key quantities that lend insight into the fundamental system transport aspects that provide valuable and crucial information for nanoscale elements in superconducting spintronics devices, as described in the introduction. Under equilibrium conditions, the vector charge ($\vec{J}^c$) and spin ($\vec{J}^{s\gamma}$) current densities can be expressed by the Keldysh block as follows:[47,78]

$$\vec{J}^c(\boldsymbol{r},\varphi)=J^c_0\left|\int_{-\infty}^{+\infty}d\varepsilon\text{Tr}\Big\{\hat{\rho}_3\big(\check{G}(\boldsymbol{r})[\check{\partial},\check{G}(\boldsymbol{r})]\big)^K\Big\}\right|, \tag{10}$$

$$\vec{J}^{s\gamma}(\boldsymbol{r},\varphi)=J^s_0\left|\int_{-\infty}^{+\infty}d\varepsilon\text{Tr}\Big\{\hat{\rho}_3\nu^\gamma\big(\check{G}(\boldsymbol{r})[\check{\partial},\check{G}(\boldsymbol{r})]\big)^K\Big\}\right|, \tag{11}$$

where $J^c_0=N_0eD/4$, $J^s_0=\hbar J^c_0/2e$, and N_0 is the number of states at the Fermi surface. The vector current densities determine the local direction and amplitude of the currents as a function of coordinates inside the F strip. In other words, $\vec{J}(\boldsymbol{r})$, provides a spatial map to the currents inside the system. We designate $\gamma=x,y,z$ for the three components of spin current, $\vec{J}^{s\gamma}$. The matrices we use throughout our derivations are given in Appendix A. To obtain the total Josephson charge current flowing through the magnetic strip, an additional integration over the y direction should be performed on Eq. (10) (see Fig. 1). The spin-dependent fields yield lengthly and cumbersome expressions, the details of which are not presented here for clarity. Having now outlined the theoretical

approach utilized in this paper, we can now present our findings in the next section.

III. RESULTS AND DISCUSSIONS

In our computations below, we consider a uniform and coordinate-independent vector potential, $\vec{A}(\boldsymbol{r})$, i.e. $\vec{\partial}\cdot\vec{A}(\boldsymbol{r}) = 0$, so that the spin vector potential is constant in the entire F region. A specific choice for the constant spin vector potential that results in Rashba (α)[12] and Dresselhaus (β)[13] types of SOC is,

$$\begin{cases} \mathcal{A}_x^x = -\mathcal{A}_y^y = 2\beta, \\ \mathcal{A}_x^y = -\mathcal{A}_y^x = 2\alpha, \\ \hline \mathcal{A}_x^z = \mathcal{A}_y^z = 0, \\ \mathcal{A}_z^z = \mathcal{A}_z^x = \mathcal{A}_z^y = 0. \end{cases} \tag{12}$$

By substituting the above set of parameters into Eqs. (7), we arrive at,

$$A_x = \beta\tau^x - \alpha\tau^y, \tag{13a}$$
$$A_y = \alpha\tau^x - \beta\tau^y. \tag{13b}$$

The Rashba SOI[20] can be described through spatial inversion asymmetries while the Dresselhaus SOI[13] is described by bulk inversion asymmetries in the crystal structure.[20,21] Crystallographic inversion asymmetries[87] or lack of structural inversion symmetries[16,17,84,87] in heterostructures may cause the ISOIs considered here. For example, strain can induce such inversion asymmetries[43,87,92,93] and thus, ISOIs, or the adjoining of two differing materials may generate the requisite interfacial SOIs[16,17,73,84,87]. Nonetheless, there is no straightforward method to measure SOIs in a hybrid structure. One possible approach would be first principle calculations[85] in conjunction with spin transfer torque experiments[73,86,87]. The intrinsic SOIs are often given by the first-order quasiparticle momentum, which is locked to their spins. This linearized approach is a simplification to the more generic picture dealing with higher orders of momentum,[21,82,92–95] which can be observed in e.g., engineered materials.[92,93] We here assume that ISOCs can be described by linear terms in the carriers' momentum.[13,20] Candidate materials to support spontaneous broken time-reversal and broken inversion symmetries include electron liquids with ISOIs, which naturally tend to have a Stoner-type magnetism at low densities, and a magnetically doped topological insulator surface (or by directly coating a topological insulator surface with magnetic insulators).[88–90] Other promising candidates involve the ferromagnetic semiconductors (Ga,Mn)As, where both the electronic structure and inherent magnetism make these materials well suited for experimental studies.[7,8,91] Our quasiclassical approach allows us to study systems involving nontrivial magnetizations and spin vector potentials with arbitrary spatial patterns. We thus consider a finite-sized, uniformly magnetized F wire whose exchange field can take arbitrary orientations. In order to determine systematically the behaviors of the spin and charge currents, we consider three orthogonal magnetization directions, namely along the x, y, and z axes. In addition, we incorporate pure Rashba ($\alpha \neq 0, \beta = 0$) and Dresselhaus ($\beta \neq 0, \alpha = 0$) SOCs that allow isolation of their effects relative to the physical quantities under study. When finding solutions to the Usadel equation, Eq. (2), and the corresponding current densities [Eqs. (10) and (11)], we have added a small imaginary part, $\delta \approx 0.01\Delta_0$, to the quasiparticles' energy, $\varepsilon \to \varepsilon + i\delta$, to enhance stability of the numerical solutions. The imaginary part can be physically viewed as accounting for inelastic scatterings.[68] Due to the presence of the finite parameter δ, we take the modulus of the currents in Eqs. (10) and (11). We normalize the quasiparticles' energy, ε, and exchange field $\vec{h}$ by the gap, Δ_0, at $T = 0$. Also, all lengths are measured in units of the superconducting coherence length ξ_S. In our computations, we adopt natural units, so that $k_B = \hbar = 1$.

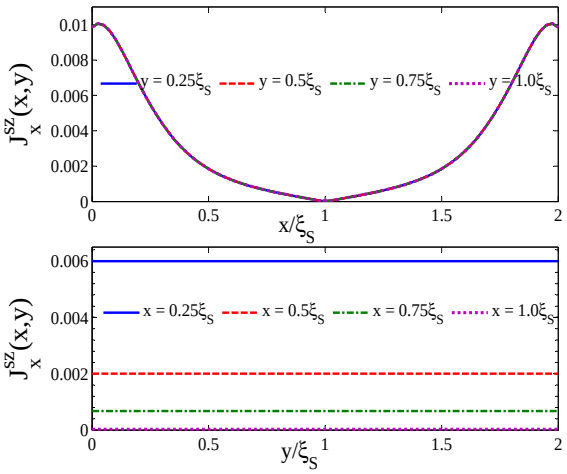

FIG. 2. (Color online) Spatial profile of the spin current in a uniformly magnetized $S/F/S$ Josephson (see Fig. 1) junction without ISOI. The magnetic exchange field is oriented along z, $\vec{h} = (0, 0, h^z)$, and therefore, solely the z component of spin current $J_x^{sz}(x, y)$ is nonvanishing. The junction length and width are set to $d_F = 2.0\xi_S$ and $W_F = 2.0\xi_S$, respectively. The top panel exhibits the spin current variations along the x-position (the junction length) at four differing locations along the junction width, $y = 0.25\xi_S, 0.5\xi_S, 0.75\xi_S, 1.0\xi_S$. The bottom panel shows $J_x^{sz}(x, y)$ as a function of y-position along the junction width, at $x = 0.25\xi_S, 0.5\xi_S, 0.75\xi_S, 1.0\xi_S$.

To begin, we consider for comparison purposes, an $S/F/S$ Josephson junction in the absence of SOCs.[28,29] The schematic of the $S/F/S$ structure is depicted in Fig. 1. The parameters $\zeta = 4$, $|\vec{h}| = 10\Delta_0$ and $d_F = 2.0\xi_S$, ensure the validity of low proximity limit considered throughout the paper. To have absolute comparisons, we set $\vec{h} = (0, 0, h^z)$ and compute the charge and spin currents using Eqs. (10) and (11), respectively. Figure 2 exhibits the spatial map of the spin current for $W_F = 2.0\xi_S$ (see Fig. 1). Since the magnetization orientation is fixed along the z direction, $J_x^{sz}(x, y = y_0)$ is the only nonvanishing component of spin current for a given fixed location y_0. The top panel of Fig. 2 illustrates the spatial variations of $J_x^{sz}(x, y = y_0)$ along the junction length in the x direction

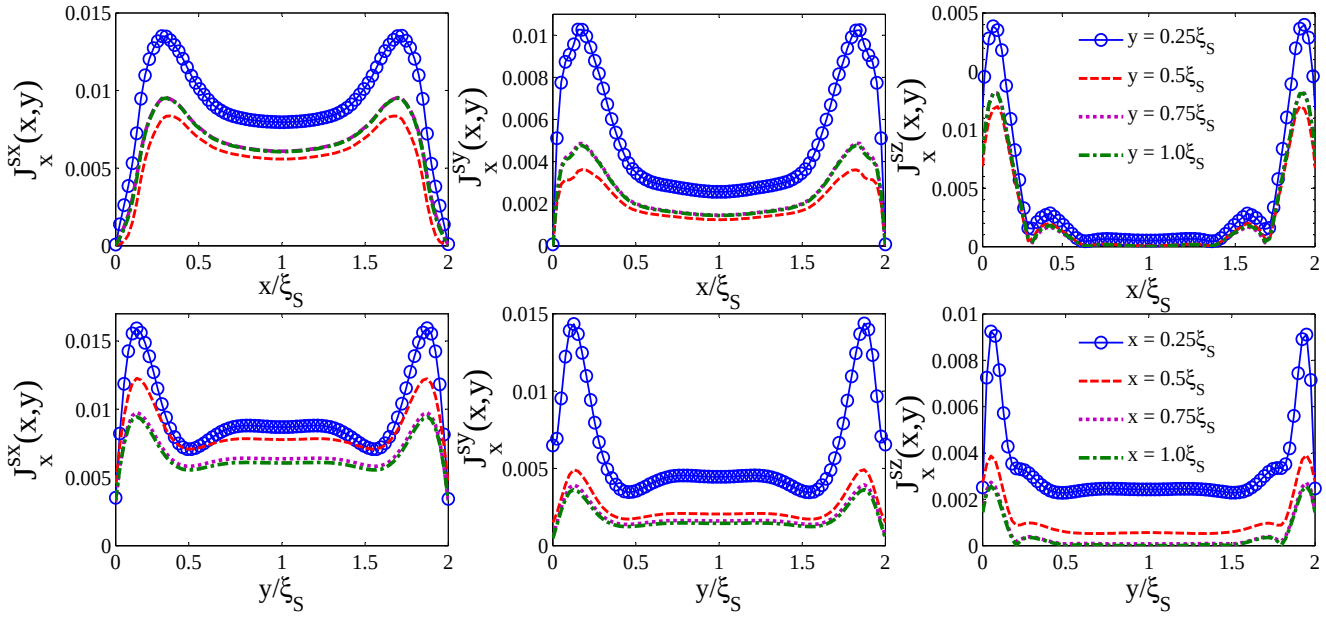

FIG. 3. (Color online) Spatial behavior of the three spin current components, $J_x^{sx}(x,y)$, $J_x^{sy}(x,y)$, and $J_x^{sz}(x,y)$ in a uniformly magnetized Rashba $S/F/S$ junction. The exchange field of the ferromagnetic strip points along the z direction: $\vec{h} = (0,0,h^z)$ (see Fig. 1). The panels in the top row show the spin current components, $J_x^{s\gamma}(x,y)$, as a function of x at four differing locations along the junction width: y=0.25ξ_S, 0.5ξ_S, 0.75ξ_S, and 1.0ξ_S. The bottom row exhibits $J_x^{s\gamma}(x,y)$ versus y at x=0.25ξ_S, 0.5ξ_S, 0.75ξ_S, and 1.0ξ_S.

at differing positions along the junction width: $y_0 = 0.25\xi_S$, $0.5\xi_S$, $0.75\xi_S$, and $1.0\xi_S$. The macroscopic phase difference between the S electrodes is set at a representative value, i.e., $\varphi = \pi/2$. The bottom panel in Fig. 2 shows $J_x^{sz}(x = x_0, y)$ as a function of y, at $x_0 = 0.25\xi_S, 0.5\xi_S, 0.75\xi_S, 1.0\xi_S$. The results demonstrate that the spin current is y independent in such hybrid junctions, namely $J_x^{sz}(x = x_0, y) = const.$ (we also have found $J_y^{sz}(x,y) = 0$). In other words, it is appropriate to view this type of system as an effectively one-dimensional junction. The variation of $J_x^{sz}(x,y)$ along the x direction is a consequence of spin torque transfer, and hence the spin current is not a conserved quantity.[44,45,47,59] The spin current is maximal at the S/F interfaces and vanishes at the middle of junction, $x = 1.0\xi_S = d_F/2$. This is contrast to the charge supercurrent in the F region, which is conserved, and thus has a constant value within the entire F strip (not shown).

To identify some of the salient features in Fig. 2, we consider now a simplified one-dimensional $S/F/S$ system, which permits analytical expressions for the spin current density. To this end, we linearize the Usadel equation, and incorporate the Kupriyanov boundary conditions, where the superconducting electrodes have strong scattering impurities. We also still assume that the magnetization is oriented along z: $\vec{h} = (0,0,h^z)$. Correspondingly, we define the dimensionless quantity, $\lambda_\pm = 2i(\varepsilon \pm h^z)/\varepsilon_T$, in which ε_T is the Thouless energy, and the dimensionless x coordinate, $\tilde{x} = x/d_F \in [0,1]$. After some straightforward calculations, we obtain the following expression for the charge current [Eq. (10)]:

$$J_x^c(x,\varphi) = J_0^c \sin\varphi \int_{-\infty}^{+\infty} d\varepsilon \frac{2i\tanh(\varepsilon k_B T/2)}{\zeta^2 \lambda_+ \lambda_-} \Big\{ [s^*(-\varepsilon)]^2 \Big(\lambda_+ \csc\lambda_- + \lambda_- \csc\lambda_+\Big) + [s^*(\varepsilon)]^2 \Big(\lambda_+ \mathrm{csch}\lambda_- + \lambda_- \mathrm{csch}\lambda_+\Big)\Big\}. \tag{14}$$

The charge current in this case is seen to exhibit the usual $\sin\varphi$ odd-functionality in the superconducting phase difference. Likewise, by substituting the solutions into Eq. (11), we arrive at the following expressions for the spin current components:

$$J_x^{sx}(x,\varphi) \equiv 0, \tag{15a}$$

$$J_x^{sy}(x,\varphi) \equiv 0, \tag{15b}$$

$$J_x^{sz}(x,\varphi) = J_0^s \int_{-\infty}^{+\infty} d\varepsilon \frac{2\tanh(\varepsilon k_B T/2)}{\zeta^2 \lambda_+ \lambda_-} \Big\{ [s^*(\varepsilon)]^2 \lambda_+ \cosh 2\tilde{x}\lambda_- \mathrm{csch}\lambda_- \cos\varphi + [s^*(-\varepsilon)]^2 \Big(\lambda_+ \csc^2\lambda_- (\cos\lambda_- + \cos\varphi)\sin[\lambda_-(1-2\tilde{x})] - \lambda_- \csc^2\lambda_+ (\cos\lambda_+ + \cos\varphi)\sin[\lambda_+(1-2\tilde{x})]\Big) + [s^*(\varepsilon)]^2 \Big(\lambda_+ \coth\lambda_- \mathrm{csch}\lambda_- (\sinh[\lambda_-(1-2\tilde{x})] - \sinh 2\tilde{x}\lambda_- \cos\varphi) - \lambda_- \mathrm{csch}^2\lambda_+ (\cosh\lambda_+ + \cos\varphi)\sinh[\lambda_+(1-2\tilde{x})]\Big)\Big\}. \tag{15c}$$

Equations (15a)-(15c) clearly demonstrate that the only nonvanishing component of spin current is J_x^{sz}, which is consistent with the exchange field aligned along z.[75] From Eq. (15c), it is also evident that J_x^{sz} is an odd function of the coordinate $\tilde{x}$ relative to the middle of the junction (and thus vanishes there), and an even function of the phase difference, φ. These features are entirely consistent with the numerical results seen in Fig. 2.

We now incorporate Rashba and Dresselhaus SOCs, while keeping the magnetization orientation intact along the z direction. The ISOIs are confined within the F region and are not present within the S electrodes. Through exhaustive numerical investigations, we have found several symmetries among the components of spin current (discussed below) at three particular directions of the exchange field. Due to the symmetries available among the spin current components, we focus here on Rashba SOC. We emphasize that similar conclusions can be drawn for Dresselhaus SOC through the symmetries described below. Figure 3 exhibits the spatial profiles for the spin current density components, $J_x^{sx}(x,y)$, $J_x^{sy}(x,y)$, and $J_x^{sz}(x,y)$. A square ferromagnetic strip is considered, with $d_F = W_F = 2.0\xi_S$, and the superconducting phase difference is equal to $\varphi = \pi/2$. The Rashba SOC coefficient is set to a representative value $\alpha = 2.0\xi_S$, without loss of generality.[73] The top set of panels show $J_x^{s\gamma}(x, y = y_0)$ [$\gamma = x, y, z$] as a function of the x coordinate at $y_0 = 0.25\xi_S$, $0.5\xi_S$, $0.75\xi_S$, and $1.0\xi_S$. Whereas the bottom panels represent the same quantities, but now as a function of y at $x_0 = 0.25\xi_S$, $0.5\xi_S$, $0.75\xi_S$, and $1.0\xi_S$. As seen in Fig. 1, the junction length and width are parallel to the x and y axes, respectively. The components $J_x^{sx}(x, y = y_0)$ and $J_x^{sy}(x, y = y_0)$, shown in the top row of Fig. 3, demonstrate that these spin current densities vanish at the S/F contacts. This finding is consistent with previous works involving nonsuperconducting heterojunctions[43–45,47,67]. The z component, $J_x^{sz}(x, y = y_0)$, however exhibits opposite behavior, and is nonzero at the S/F contacts due to the exchange field, which is oriented along the z axis. Similarly, as seen in Fig. 2, $J_x^{sz}(x, y = y_0)$ is finite at the S/F interfaces near the S reservoirs. One of the most important features of the results is seen in the top panels of Fig. 3, where two peaks in $J_x^{s\gamma}(x, y)$ emerge near the S/F contacts. We restrict the spatial profiles to $0 < x < d_F/2$ and $0 < y < W_F/2$, since the results are symmetrical with respect to $x = 1.0\xi_S = d_F/2$ and $y = 1.0\xi_S = W_F/2$, so that the maxima of $J_x^{s\gamma}(x, y = y_0)$ occurs near the edges of the F wire [at $x = 0$, and $x = d_F$]. Turning to the bottom row of panels in Fig. 3, we see that $J_x^{s\gamma}(x = x_0, y)$ are nonzero at the vacuum boundaries, $y = 0$, and $y = W_F$. Here also the largest values in the spin current density components take place near the transverse edges of the F wire ($y = 0$, and $y = W_F$). The magnitude of the spin current densities at $x = 0.25\xi_S$ are generally larger than the other x positions, in agreement with the results of $J_x^{s\gamma}(x, y = y_0)$ shown in the top row of panels.

We now consider the effects of changing the magnetization alignment in the ferromagnet. Thus, Fig. 4 represents the same Rashba spin-orbit coupled $S/F/S$ junction as in Fig. 3, except the magnetization of the F wire is now oriented along the y axis. This specific direction of $\vec{h}$ leads to $J_x^{sx}(x, y = y_0) = J_x^{sz}(x, y = y_0) = 0$ at the S/F interfaces and the spin current densities peak near the edges of F wire. The spin current density $J_x^{sy}(x, y = y_0)$ however is nonzero at the S/F contacts similarly to $J_x^{sz}(x, y = y_0)$ in the configuration where the magnetization points along the z direction (Fig. 3). As mentioned earlier, this nonvanishing behavior is directly related to the exchange field direction which lies now parallel to the y axis. Examining $J_x^{s\gamma}(x = x_0, y)$ in the bottom row panels in Fig. 4, the maximal values of $J_x^{s\gamma}(x = x_0, y)$ take place near the vacuum boundaries, i.e. $y = 0$, and $y = W_F$. Our investigations demonstrate similar qualitative trends for the components of $J_x^{s\gamma}(x = x_0, y)$ when the magnetization resides along the x axis. Note that the transverse components of the spin currents are nonzero inside the ISO coupled ferromagnetic wire, i.e., $J_y^{s\gamma}(x, y) \neq 0$, and vanish at the vacuum boundaries ($y = 0, W_F$). We mainly focus here on the $J_x^{s\gamma}(x, y)$, since the longitudinal components contain the relevant information needed to describe and understand the accumulation of spin current densities at the edges of the structures.

Considering now the previous characterization of the spin current components in systems with ISOCs, we schematically summarize the spatial maps in Fig. 5 for $\vec{J}^{s\gamma}(x, y)$. The largest amplitudes of $\vec{J}^{s\gamma}(x, y)$ reside near the edges of the F strip, i.e. $x = 0, d_F$ and $y = 0, W_F$. We have qualitatively marked these regions by light yellow "ribbons". Therefore, the overlap of maximal amplitudes take place near the corner regions of the F strip. We have marked these areas by dashed curves and with a deeper yellow color. The spatial profiles found here are qualitatively similar to the existence of edge spin currents found in nonsuperconducting heterojunctions with ISOIs,[39–46] except with one crucial difference: here spin accumulation at the edges arises in the absence of an external field. As mentioned in other works[67], the spin accumulation is a signature of the spin Hall effect. Therefore, the predicted spin accumulation in this paper might be measurable through optical experiments[43], such as through Kerr rotation microscopy[43], where spatial profiles of the spin polarizations near the edges can be imaged. An alternate experimental proposal involves multiterminal devices[44,45]. When transverse leads are attached to the lateral edges of a two-dimensional $S/F/S$ junction (borders at $y = 0$, $y = W_N$ in Fig. 1(a)), the spin accumulations at the F wire's edges inject spin currents into the leads.[44,45] The transversely injected spin currents into the lateral leads in turn may induce a voltage drop between the additional leads.[44,45]

The Josephson effect is a significant example of a macroscopic quantum phenomenon and is of fundamental importance in determining the properties of dissipationless coherent transport. Thus, the behavior of the spin currents upon varying the macroscopic phase difference is crucial to experiments and applications utilizing spin-Hall effects and spin transport. In Fig. 6, we therefore study the spin current components as a function of the macroscopic phase difference, φ, between the S banks. We consider the parameter set used in Fig. 4, including $\vec{h} = (0, h^y, 0)$. In the top set of panels, the spatial variations of $J_x^{s\gamma}(x, y)$ are plotted at $\varphi = 0$, 0.2π, 0.4π, and

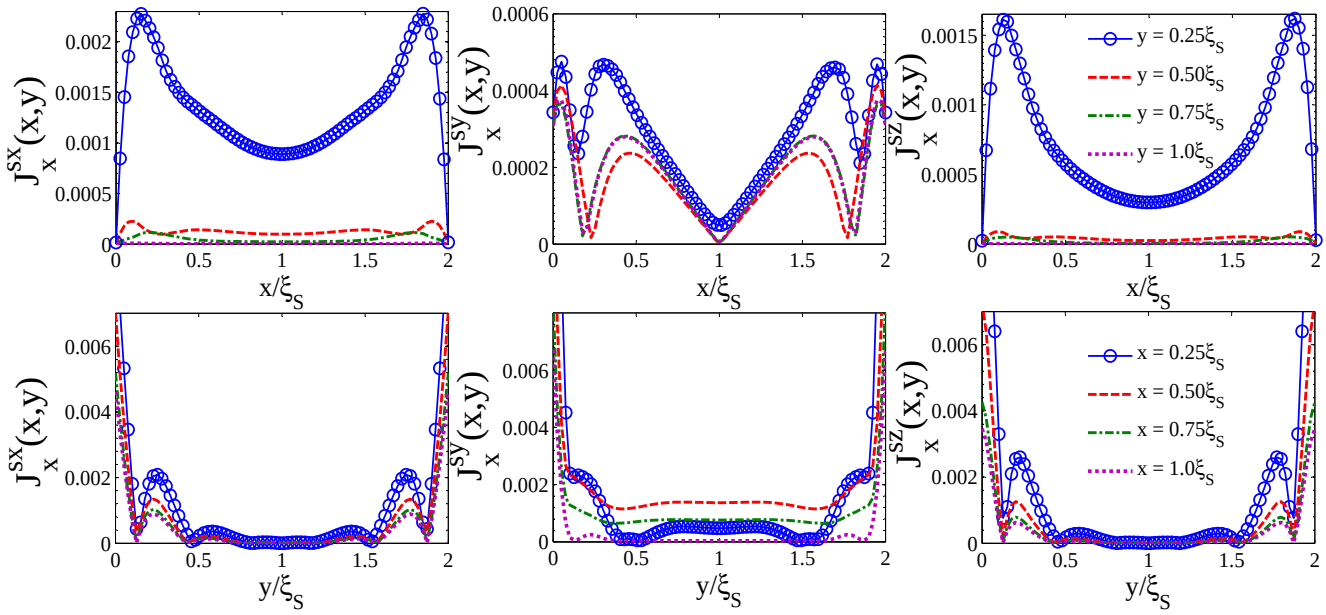

FIG. 4. (Color online) Spatial profiles of the spin current components; $J_x^{sx}(x,y)$, $J_x^{sy}(x,y)$, and $J_x^{sz}(x,y)$ in an $S/F/S$ system. The Rashba ferromagnetic wire's width and length are equal to $W_F = d_F = 2.0\xi_S$. The exchange field of the ferromagnetic strip is fixed along the y direction, $\vec{h} = (0, h^y, 0)$. *Top row*: spatial behavior of $J_x^{s\gamma}(x,y)$ along the junction length, x, at $y = 0.25\xi_S, 0.5\xi_S, 0.75\xi_S, 1.0\xi_S$. *Bottom row*: spatial variations of $J_x^{s\gamma}(x,y)$ along the junction width in the y direction at $x = 0.25\xi_S, 0.5\xi_S, 0.75\xi_S, 1.0\xi_S$.

1.0π. We have also chosen a representative position along the junction width, corresponding to $y = 1.0\xi_S = W_F/2$, which simplifies the analysis while maintaining the generality of the discussion. Although $J_x^{s\gamma}(x,y)$ has a minimum at $y = 1.0\xi_S$, it exhibits the same trends as a function of φ compared to the other positions inside the F wire. By increasing the superconducting phase difference from 0 to π, the amplitudes of the spin current components decrease overall. In the bottom set of panels of Fig. 4, we illustrate $\langle J_x^{s\gamma}(x,y)\rangle_x$ as a function of φ, at $y = 0.25\xi_S$, $0.5\xi_S$, $0.75\xi_S$, and $1.0\xi_S$. Here, we denote the spatial average over the x coordinate from 0 to d_F by $\langle ...\rangle_x$. In order to better visualize the averaged profiles, we use logarithmic scales in the vertical axes of the bottom row of panels. As seen, the three components of spin current $\langle J_x^{s\gamma}(x,y)\rangle_x$ are even-functions of φ, with a period of 2π, namely $J^{s\gamma}(2n\pi + \varphi) = J^{s\gamma}(-\varphi)$, $n \in \mathbb{Z}$. This is contrary to the charge supercurrent which is an odd-function of φ, i.e., $J^c(2n\pi + \varphi) = -J^c(-\varphi)$ regardless of a finite phase-shift φ_0[66,69,70]. These findings are entirely consistent with previous studies of $S/F/S$ Josephson junctions with inhomogeneous magnetization patterns[68]. We here remark that an additional phase-shift φ_0 may appear in such junctions due to the coupling of exchange field and ISOIs.[66,69,70] Nonetheless, the explicit current-phase relations simply undergo a shift in φ_0.[66,69] According to the current-phase relations, the charge supercurrent vanishes at certain φ that is quite different than the behavior of the spin current components which clearly show nonzero values at the same φ. Therefore, these differences in charge and spin currents allows for an examination of edge spin currents without any net charge current in an ISO coupled F wire sandwiched between two S banks.

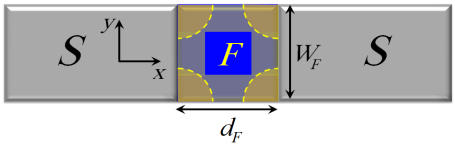

FIG. 5. (Color online) Qualitative illustration of the edge spin current densities in a Rashba or Dresselhaus spin-orbit coupled $S/F/S$ junction. The light yellow ribbons display edge regions with maximum spin current densities. The induced spin currents can be considered as a response of the intrinsic spin-orbit coupled system to the presence of an exchange field (the combination of spontaneously broken time-reversal symmetries and the lack of inversion symmetries). As shown in Fig. 1, the exchange field of the ferromagnetic wire is uniform and can take arbitrary directions. The regions that carry maximal accumulation of spin currents are qualitatively shown by the semicircular regions.

We are now in a position to discuss symmetries that may arise among the spin current density components for differing magnetization orientations in systems with either Rashba or Dresselhaus SOCs. Our investigations have found that the out-of-plane spin current, $\vec{J}^{sz}(x,y)$, remains unchanged upon exchanging the Rashba and Dresselhaus SOCs, regardless of the magnetization orientation. This follows from the form of the spin vector potential discussed at the beginning of this section. However, this picture changes for the in-plane $\vec{J}^{s\{x,y\}}(x,y)$ components. The x and y components of the spin current become interchanged when transforming from one type of spin-orbit interaction to another. Precisely speaking, by going from Rashba to Dresselhaus spin-orbit coupling,

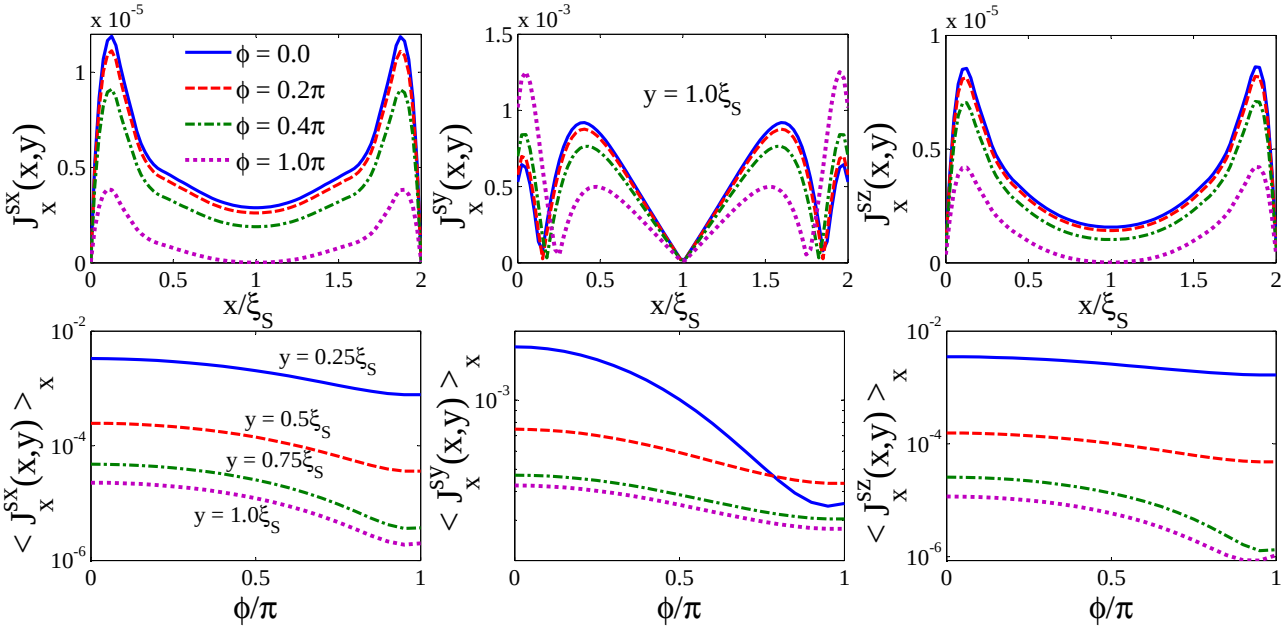

FIG. 6. (Color online) Spin current components for differing values of the superconducting phase difference φ in a Rashba spin-orbit coupled $S/F/S$ Josephson junction. The top row of panels shows the spatial variations of $J_x^{s\gamma}(x,y)$ as a function of x along the junction length at $\varphi = 0, 0.2\pi, 0.4\pi$, and 1.0π. The location along the junction width is fixed at the middle of the junction, $y = W_F/2 = 1.0\xi_S$. The bottom row of panels represents the spatially averaged spin current components over the junction length (denoted by $\langle J_x^{s\gamma}(x,y)\rangle_x$) vs φ. The average is performed along four positions: y=$0.25\xi_S$, $0.5\xi_S$, $0.75\xi_S$, and $1.0\xi_S$. The ferromagnetic wire is a square strip with $d_F = W_F = 2.0\xi_S$, and exchange field $\vec{h} = (0, h^y, 0)$.

one simply needs to exchange indices x and y in the components of both the exchange field and the spin current. Otherwise, everything stays the same. By making use of the simple transformation rules described, one can easily deduce the results of Dresselhaus spin-orbit coupled systems from the plots presented for Rashba spin-orbit coupled $S/F/S$ systems shown in Figs. 3, 4, and 6.

To conclude this section, we briefly discuss the importance of having a magnetic element in the Josephson junction for the effect of spin current edge accumulation to take place spontaneously. We thus take the limiting case of $\vec{h} = 0$ in our previous calculations above involving $S/F/S$ junctions. Using otherwise the same geometrical and material parameters, this case was found to produce no spin current, $\vec{J}^{s\gamma}(x,y) = 0$, in the presence of Rashba ($\alpha \neq 0, \beta = 0$) and/or Dresselhaus ($\beta \neq 0, \alpha = 0$) SOIs. These findings are consistent with previous works,[67] where several simplifying approximations were employed for Rashba-based $S/N/S$ systems. Examining also the charge supercurrent, $\vec{J}^c(x,y)$, for both the Rashba and Dresselhaus interactions, we observed a uniform spatial map for the charge current density for all φ, with $J_x^c = const.$, and $J_y^c = 0$. In other words, the spin-dependent fields cannot induce transverse charge supercurrents in a diffusive $S/N/S$ junction. This is in stark contrast to its ballistic $S/N/S$ counterpart, where a transverse charge supercurrent (that is, equivalent to a supercurrent flowing along the y direction in our configuration depicted in Fig. 1) was theoretically predicted due to the presence of intrinsic SOIs[83].

IV. CONCLUSIONS

We have theoretically studied the behavior of spin and charge currents in a finite-size two-dimensional $S/F/S$ Josephson junction with intrinsic spin-orbit couplings. We utilized a two-dimensional Keldysh-Usadel quasiclassical approach that incorporates a generic spin-dependent vector potential. Our results demonstrate that the combination of a uniform magnetization and ISOIs drives the spin currents which spontaneously accumulate at the F wire's edges. The corners of the F wire were shown to host the maximum density of spin currents. (As demonstrated in Ref. 75, similar edge phenomena can be found in finite-size two-dimensional intrinsically spin orbit coupled $S/N/S$ junctions with a single spin active interface. Additionally, it was shown that maximum singlet-triplet conversions take place at the corners of N wire nearest the spin active interfaces[75].) Our investigations show that the spontaneous edge accumulation of the spin currents are robust and can exist at all magnetization orientations, independent of the actual type of ISOIs. Our investigations have also found several symmetries among the spin current components upon varying magnetization orientations coupled to a Rashba or Dresselhaus SOI. By varying the superconducting phase difference, φ, between the S banks, we determined the spin and charge currents as a function of phase difference. We have found that net spin currents therefore emerge and accumulate spontaneously at the edges, in the absence of charge flow, when properly modulating φ in finite-size two-dimensional intrinsically spin-orbit coupled $S/F/S$ hybrid structures. This

work can be viewed as complementary to previous studies involving edge spin currents in non-superconducting spin-orbit coupled structures where externally imposed fields were required[42–45,47,50,67]. We have shown that remarkably, edge spin currents can be spontaneously driven by the coupling of intrinsic properties of a system, i.e. spontaneously broken time-reversal and the lack of inversion symmetries in the *absence* of any externally imposed field.

ACKNOWLEDGMENTS

We would like to thank G. Sewell for helpful discussions in the numerical parts of this work. We also thank F.S. Bergeret for valuable comments, suggestions, and numerous discussions which helped us to improve the manuscript. K.H. is supported in part by ONR and by a grant of supercomputer resources provided by the DOD HPCMP.

Appendix A: Pauli Matrices

In Sec. II we introduced the Pauli matrices in the spin space and denoted them by $\vec{\sigma} = \left(\sigma^x, \sigma^y, \sigma^z\right)$, $\vec{\tau} = \left(\tau^x, \tau^y, \tau^z\right)$, and $\vec{\nu} = \left(\nu^x, \nu^y, \nu^z\right)$.

$$\sigma^x = \begin{pmatrix} 0 & 1 \\ 1 & 0 \end{pmatrix},\ \sigma^y = \begin{pmatrix} 0 & -i \\ i & 0 \end{pmatrix},\ \sigma^z = \begin{pmatrix} 1 & 0 \\ 0 & -1 \end{pmatrix},\ \sigma^0 = \begin{pmatrix} 1 & 0 \\ 0 & 1 \end{pmatrix}.$$

We also introduced the 4×4 matrices $\vec{\hat{\rho}} = (\hat{\rho}_1, \hat{\rho}_2, \hat{\rho}_3)$:

$$\hat{\rho}_1 = \begin{pmatrix} 0 & \sigma^x \\ \sigma^x & 0 \end{pmatrix},\ \hat{\rho}_2 = \begin{pmatrix} 0 & -i\sigma^x \\ i\sigma^x & 0 \end{pmatrix},\ \hat{\rho}_3 = \begin{pmatrix} \sigma^0 & 0 \\ 0 & -\sigma^0 \end{pmatrix}.$$

Following Ref. 68, we define τ^γ, ν^γ, and $\hat{\rho}_0$ as follows;

$$\tau^\gamma = \begin{pmatrix} \sigma^\gamma & 0 \\ 0 & \sigma^\gamma \end{pmatrix},\ \nu^\gamma = \begin{pmatrix} \sigma^\gamma & 0 \\ 0 & \sigma^{\gamma *} \end{pmatrix},\ \hat{\rho}_0 = \begin{pmatrix} \sigma^0 & 0 \\ 0 & \sigma^0 \end{pmatrix},$$

to unify our notation throughout the paper γ stands for x, y, z.

* phymalidoust@gmail.com
† klaus.halterman@navy.mil

[1] G.A. Prinz, Science **282**, 1660 (1998).
[2] J.M. Kikkawa, and D.D. Awschalom, Nature **397**, 139 (1999); D.D. Awschalom, and J.M. Kikkawa, Phys. Today **52**(6), 33 (1999).
[3] S.A. Wolf, D.D. Awschalom, R.A. Buhrman, J.M. Daughton, S. von Moln r, M.L. Roukes, A.Y. Chtchelkanova, D.M. Treger, Science **294**, 1488 (2001).
[4] S. Murakami, N. Nagaosa, S. Zhang, Science **301**, 1348 (2003).
[5] S.Q. Shen, Phys. Rev. B**70**, 081311(R) (2004).
[6] P. Sharma, Science **307**, 531 (2005).
[7] J.D. Sau, R.M. Lutchyn, S. Tewari, and S.D. Sarma, Phys. Rev. Lett. **104**, 040502 (2010).
[8] R.M. Lutchyn, J.D. Sau, and S.D. Sarma, Phy. Rev. Lett. **105**, 077001 (2010).
[9] J. Alicea, Y. Oreg, G. Refael, F.V. Oppen, M.P.A. Fisher, Nat. Phys. **7**, 412 (2011).
[10] V. Mourik, K. Zuo, S.M. Frolov, S.R. Plissard, E.P.A.M. Bakkers, and L.P. Kouwenhoven, Science **336**, 1003 (2012).
[11] F. Pientka, L. Jiang, D. Pekker, J. Alicea, G. Refael, Y. Oreg, and F.V. Oppen, New J. Phys. **15**, 115001 (2013).
[12] Y.L. Bychkov and E.I. Rashba, J. Phys. C **17**, 6093 (1984).
[13] G. Dresselhaus, Phys. Rev. **100**, 580 (1955).
[14] R.S. Popovic, *Hall Effect Devices* (Institute of Physics, Bristol, UK, ed. 2, 2004).
[15] J. Wunderlich, B. Park, A.C. Irvine, L.P. Zarbo, E. Rozkotova, P. Nemec, V. Novak, J. Sinova, and T. Jungwirth, Science **330**, 1801 (2010).
[16] I.M. Miron, G. Gaudin, S. Auffret, B. Rodmacq, A. Schuhl, S. Pizzini, J. Vogel, and P. Gambardella, Nat. Mat. **9**, 230 (2010).
[17] K. Garello, I.M. Miron, C.O. Avci, F. Freimuth, Y. Mokrousov, S. Blugel, S. Auffret, O. Boulle, G. Gaudin, and P. Gambardella, Nat. Nanotech. **8**, 587 (2013).
[18] J. Nitta, T. Akazaki, H. Takayanagi, and T. Enoki, Phys. Rev. Lett.**78**, 1335 (1997).
[19] D. Grundler, Phys. Rev. Lett.**84**, 6074 (2000).
[20] H.A. Engel, E.I. Rashba, and B.I. Halperin, *Handbook of Magnetism and Andvanced Magnetic Materials*, edited by H. Kronmuller and S. Parkin (Wiley, Chichester, UK, 2007).
[21] R. Winkler, *Spin-orbit coupling effects in two-dimensional electron and hole systems*, Springer-Verlag, 2003.
[22] D. Awschalom, N. Samarth, and D. Loss, *Semiconductor spintronics and quantum computation*, Springer, New York, 2002.
[23] Y. Asano, Y. Tanaka, M. Sigrist, and S. Kashiwaya, Phys. Rev. B**67**, 184505 (2003).
[24] S.I. Erlingsson, J. Schliemann, and D. Loss, Phys. Rev. B **71**, 035319 (2005).
[25] H. Dery, P. Dalal, L. Cywinski, and L.J. Sham, Nature **447**, 573 (2007).
[26] W.L. Lee, S. Watauchi, V.L. Miller, R.J. Cava, and N.P. Ong, Science **303**, 1647 (2004).
[27] D. Stepanenko and N.E. Bonesteel, Phys. Rev. Lett.**93**, 140501 (2004).
[28] F.S. Bergeret, A.F. Volkov, and K.B. Efetov, Rev. Mod. Phys. **77**, 1321 (2005).
[29] A.I. Buzdin, Rev. Mod. Phys.**77**, 935 (2005).
[30] T. Kontos, M. Aprili, J. Lesueur, and X. Grison, Phys. Rev. Lett. **86**, 304 (2001).
[31] T.S. Khaire, M.A. Khasawneh, W.P. Pratt, Jr., N.O. Birge, Phys. Rev. Lett. 104, 137002 (2010); K.M. Boden, W.P. Pratt Jr., and N.O. Birge, Phys. Rev. B**84**, 020510(R) (2011).
[32] M. Alidoust, K. Halterman, and J, Linder, Phys. Rev. B **88**, 075435 (2013); M. Alidoust, and K. Halterman, Phys. Rev. B **89**, 195111 (2014); M. Alidoust, and K. Halterman, Appl. Phys. Lett. **105**, 202601 (2014); M. Alidoust, and K. Halterman, J. Appl.

Phys. **117** , 123906 (2015).

[33] Ya.V. Fominov, A.F. Volkov, and K.B. Efetov, Phys. Rev. B **75**, 104509 (2007).

[34] I. Sosnin, H. Cho, V. Petrashov, A. F. Volkov, Phys. Rev. Lett. **96**, 157002 (2006).

[35] A. Cottet, D. Huertas-Hernando, W. Belzig, and Y.V. Nazarov, Phys. Rev. B **80**, 184511 (2009); M. Eschrig, T. Lofwander, T. Champel, J.C. Cuevas, J. Kopu, and G. Schon, J. Low Temp. Phys. **147**, 457, (2007).

[36] J.W.A. Robinson, J.D.S. Witt, M.G. Blamire, Science **329**, 5987 (2010); M. Alidoust and J. Linder, Phys. Rev. B**82**, 224504 (2010); M. Alidoust, K. Halterman, J. Linder, Phys. Rev. B **89**, 054508 (2014).

[37] K. Halterman, P.H. Barsic, and O.T. Valls Phys. Rev. Lett. **99**, 127002 (2007).

[38] N.G. Pugach, M.Yu. Kupriyanov, A.V. Vedyayev, C. Lacroix, E. Goldobin, D. Koelle, R. Kleiner, and A.S. Sidorenko Phys. Rev. B **80**, 134516 (2009).

[39] S. Murakami, N. Nagaosa, and S.-C. Zhang, Science **301**, 1348 (2003).

[40] J. Sinova, D. Culcer, Q. Niu, N.A. Sinitsyn, T. Jungwirth, and A.H. MacDonald, Phys. Rev. Lett.**92**, 126603 (2004).

[41] J.N. Chazalviel, Phys. Rev. B **11**, 3918 (1975).

[42] M.I. Dyakonov and V.I. Perel, Phys. Lett. **35A**, 459 (1971); J.E. Hirsh, Phys. Rev. Lett.**83**, 1834 (1999).

[43] Y.K. Kato, R.C. Myers, A.C. Gossard, and D.D. Awschalom, Science **306**, 1910 (2004); J. Wunderlich, B. Kastner, J. Sinova, and T. Jungwirth, Phys. Rev. Lett.**94**, 047204 (2005).

[44] E.G. Mishchenko, A.V. Shytov, and B.I. Halperin, Phys. Rev. Lett.**93**, 226602 (2004).

[45] B.K. Nikolic, S. Souma, L.P. Zarbo, and J. Sinova, Phys. Rev. Lett.**95**, 046601 (2005).

[46] M. Onoda and N. Nagaosa, Phys. Rev. B **72**, 081301(R) (2005).

[47] R. Raimondi, C. Gorini, P. Schwab, and M. Dzierzawa, Phys. Rev. B**74**, 035340 (2006).

[48] G. Eilenberger, Z. Phys. **214**, 195 (1968).

[49] A.G. Malshukov, C.S. Tang, C.S. Chu, and K.A. Chao, Phys. Rev. B**68**, 233307 (2003).

[50] A.G. Malshukov, S. Sadjina, and A. Brataas, Phys. Rev. B**81**, 060502(R) (2010).

[51] H. Kontani, J. Goryo, and D.S. Hirashima, Phys. Rev. Lett.**102**, 086602 (2009).

[52] L.Y. Wang, C.S. Chu, and A.G. Malshukov, Phys. Rev. B**78**, 155302 (2008).

[53] M. Cheng and R.M. Lutchyn Phys. Rev. B**86**, 134522 (2012).

[54] A. Reynoso, G. Usaj, C.A. Balseiro, D. Feinberg, and M. Avignon, Phys. Rev. B**86**, 214519 (2012).

[55] M. Franz, Physics **3**, 24 (2010).

[56] R.F. Service, Science **332**, 193 (2011).

[57] Y.C. Tao and J.G. Hu, Phys. Rev. B**72**, 165329 (2005).

[58] X. Liu, J.K. Jain, and C.X. Liu, arXiv:1312.6458

[59] A.B. Vorontsov, I. Vekhter, and M. Eschrig, Phys. Rev. Lett.**101**, 127003 (2008).

[60] I.V. Bobkova and Yu.S. Barash, JETP Lett. **80**, 494 (2004).

[61] E. Arahata, T. Neupert, and M. Sigrist, Phys. Rev. B**87**, 220504(R) (2013).

[62] E.V. Bezuglyi, A.S. Rozhavsky, I.D. Vagner, and P. Wyder, Phys. Rev. B**66**, 052508 (2002).

[63] I. Krive, S. Kulinich, R. Shekhter, and M. Jonson, Low Temp. Phys. **30**, 554 (2004); I. Krive, A.M. Kadigrobov, R. Shekhter, and M. Jonson, Phys. Rev. B, **71**, 214516 (2005).

[64] L. DellAnna, A. Zazunov, R. Egger, and T. Martin, Phys. Rev. B**75**, 085305 (2007); A. Zazunov, R. Egger, T. Jonckheere and T. Martin, Phys. Rev. Lett.**103**, 147004 (2009)

[65] B. Beri, J.H. Bardarson, and C.W.J. Beenakker, Phys. Rev. B**77**, 045311 (2008).

[66] T. Yokoyama, M. Eto, and Y.V. Nazarov, Phys. Rev. B**89**, 195407 (2014).

[67] A.G. Malshukov and C.S. Chu, Phys. Rev. B**78**, 104503 (2008).

[68] M. Alidoust, J. Linder, G. Rashedi, T. Yokoyama, and A. Sudbo, Phys. Rev. B**81**, 014512 (2010).

[69] A. I. Buzdin, Phys. Rev. Lett.**101**, 107005 (2008).

[70] F. Konschelle, arXiv:1408.4533.

[71] M. Faure, A.I. Buzdin, A.A. Golubov, and M.Y. Kupriyanov, Phys. Rev. B**73**, 064505 (2006).

[72] E.A. Demler, G.B Arnold, and M.R. Beasley, Phys. Rev. B**55**, 15174 (1997); S. Oh, Y.H. Kim, D. Youm, and M.R. Beasley, Phys. Rev. B**63**, 052501 (2000).

[73] F.S. Bergeret and I.V. Tokatly, Phys. Rev. Lett.**110**, 117003 (2013); F.S. Bergeret and I.V. Tokatly, Phys. Rev. B**89**, 134517 (2014).

[74] Z. Niu, Appl. Phys. Lett. **101**, 062601 (2012).

[75] M. Alidoust, and K. Halterman, arXiv:1502.05719

[76] M.W. Wu, J.H. Jiang, M.Q. Weng, Phys. Rep. **61** 493 (2010).

[77] P. Schwab, M. Dzierzawa, C. Gorini, and R. Raimondi, Phys. Rev. B**74**, 155316 (2006).

[78] C. Gorini, P. Schwab, R. Raimondi, and A.L. Shelankov, Phys. Rev. B**82**, 195316 (2010).

[79] M. Duckheim, D.L. Maslov, and D. Loss, Phys. Rev. B**80**, 235327 (2009).

[80] K. Usadel, Phys. Rev. Lett. **25**, 507 (1970); A.I. Larkin and Y.N. Ovchinnikov, *in Nonequilibrium Superconductivity*, edited by D. Langenberg and A. Larkin (Elsevier, Amesterdam, 1986), P. 493.

[81] A.V. Zaitsev, Zh. Eksp. Teor. Fiz. **86**, 1742 (1984) (Sov. Phys. JETP **59**, 1015 (1984); M.Y. Kuprianov etal, Sov. Phys. JETP **67**, 1163 (1988).

[82] R.S. Chang, C.S. Chu, and A.G. Malshukov, Phys. Rev. B**79** 195314 (2009).

[83] T. Yokoyama, arXiv:1107.4202

[84] M. Duckheim and P.W. Brouwer, Phys. Rev. B **83**, 054513 (2011); S. Takei and V. Galitski, Phys. Rev. B **86**, 054521 (2012); Y.M. Koroteev, G. Bihlmayer, J.E. Gayone, E.V. Chulkov, S. Blugel, P.M. Echenique, and P. Hofmann, Phys. Rev. Lett. **93**, 046403 (2004).

[85] C.R. Ast, J. Henk, A. Ernst, L. Moreschini, M.C. Falub, D. Pacile, P. Bruno, K. Kern, and M. Grioni, Phys. Rev. Lett. **98**, 186807 (2007).

[86] A. Manchon and S. Zhang, Phys. Rev. B **78**, 212405 (2008).

[87] S.D. Ganichev and L.E. Golub, Phys. Status Solidi B, **1** 23 (2014); S. Giglberger, L.E. Golub, V.V. Belkov, S.N. Danilov, D. Schuh, C. Gerl, F. Rohlfing, J. Stahl, W. Wegscheider, D. Weiss, W. Prettl, and S.D. Ganichev, Phys. Rev. B**75**, 035327 (2007).

[88] C. Xu, Phys. Rev. B **81**, 144431 (2010); Phys. Rev. B **81**, 054403 (2010).

[89] P. Wei, F. Katmis, B.A. Assaf, H. Steinberg, P. Jarillo-Herrero, D. Heiman, and J.S. Moodera, Phys. Rev. Lett. **110**, 186807 (2013); E. Berg, M.S. Rudner, and S.A. Kivelson, Phys. Rev. B **85**, 035116 (2012).

[90] M.Z. Hasan and C.L. Kane, Rev. Mod. Phys.**82**, 3045 (2010); X.-L. Qi and S.-C. Zhang, Rev. Mod. Phys.**83**, 1057 (2011)

[91] T. Jungwirth, J. Wunderlich, V. Novak, K. Olejnik, B.L. Gallagher, R.P. Campion, K.W. Edmonds, A.W. Rushforth, A.J. Ferguson, and P. Nemec Rev. Mod. Phys. **86**, 855 (2014).

[92] R. Moriya, K. Sawano, Y. Hoshi, S. Masubuchi, Y. Shiraki, A. Wild, C. Neumann, G. Abstreiter, D. Bougeard, T. Koga, and T. Machida, Phys. Rev. Lett.**113**, 086601 (2014).

[93] H. Nakamura, T. Koga, and T. Kimura, Phys. Rev. Lett. **108**, 206601 (2012).

[94] G.M. Minkov, A.A. Sherstobitov, A.V. Germanenko, O.E. Rut, V.A. Larionova, and B.N. Zvonkov, Phys. Rev. B **71**, 165312 (2005).
[95] R. Winkler, Phys. Rev. B **62**, 4245 (2000); R. Winkler, H. Noh, E. Tutuc, and M. Shayegan, Phys. Rev. B **65**, 155303 (2002).